https://doi.org/10.5194/egusphere-2026-3442
Preprint. Discussion started: 29 June 2026

Unveiling carbonate dissolution in coastal sediments and its influence on seawater buffering capacity with $\delta^{13}C_{DIC}$ and ^{224}Ra–^{228}Th disequilibria

Xinjie Ma[1,2], Xiangming Shi[1,2]*, Yingxu Wu[1,2], Xiangqi Yi[1,2], Biqi Zheng[3], Di Qi[1,2]*

[1]State Key Laboratory of Mariculture Breeding, Jimei University, Xiamen, 361021, China.

[2]Polar and Marine Research Institute, Jimei University, Xiamen, 361021, China.

[3]Ningde Marine Center, Ministry of Natural Resources, Ningde, 352000, China.

*Correspondence to: Xiangming Shi and Di Qi

Contact author: Xiangming Shi (xiangming.shi@jmu.edu.cn)

Abstract

Organic carbon mineralization is generally recognized as the primary source of dissolved inorganic carbon (DIC) released from sediments in coastal seas. The CO_2 accumulation or the formation of corrosive microenvironment induced by organic carbon degradation can promote the dissolution of calcium carbonate ($CaCO_3$) in sediments, complicating the efficiency of carbon burial and total alkalinity (TA) inputs to aquatic environments. However, quantitative assessments of sediment $CaCO_3$ dissolution and its impacts on the seawater carbonate remain poorly constrained. In this study, we selected typical high-productivity regions, mariculture farms, and applied the ^{224}Ra–^{228}Th disequilibrium approach to quantify the effluxes of DIC and TA across the sediment-water interface. Stable carbon isotopes of DIC ($\delta^{13}C_{DIC}$) were employed to trace DIC sources in porewater. The results showed that $CaCO_3$ dissolution in sediments accounted for 27–56% of the benthic DIC efflux. Notably, a high contribution of $CaCO_3$ dissolution did not coincide with strong organic carbon degradation across sites, suggesting that dynamic disturbance on sediments, which weakened the metabolic CO_2 accumulation in porewater, was also a crucial factor affecting carbonate dissolution. According to the evaluation of the influence that benthic DIC and TA efflux exerted on the seawater CO_2 content, the TA supplied by the $CaCO_3$ dissolution was identified to enhance the carbonate buffering capacity of seawater and counteracted the acidification driven by organic matter remineralization. This indicates that $CaCO_3$ dissolution in sediments should be involved in coastal carbon cycling and assessments on coastal ecosystem resilience under the risk of CO_2 elevation.

Keywords: Sediment $CaCO_3$ dissolution; DIC-$\delta^{13}C$; Benthic efflux; ^{224}Ra–^{228}Th disequilibria

https://doi.org/10.5194/egusphere-2026-3442
Preprint. Discussion started: 29 June 2026

1 Introduction

Over half of atmospheric carbon dioxide (CO_2) is estimated to be fixed by marine primary production and the coastal ocean contributes over 1.0 Pg C y^{-1} (Bauer et al., 2013; Mathis et al., 2024). Consequently, the coastal sediment becomes a crucial carbon reservoir as a result of particulate carbon deposition, particularly in high production regions such as estuaries and seaweed farms (Friedlingstein et al., 2025; Duarte et al., 2025). Some of the buried carbon undergoes early diagenetic processes, e.g., aerobic mineralization, and is transformed into dissolved inorganic carbon (DIC), reducing the long-term carbon burial (Burdige et al., 2016; Silverberg et al., 2000). For instance, approximately 35% of the deposited carbon in the surface sediment was returned to the water column in the Baltic Sea (Wakeham and Canuel, 2006); and studies in China estuaries demonstrated that DIC effluxes from sediments were in the same order of magnitude with those from the riverine or submarine groundwater discharges (Cai et al., 2015; Hong et al., 2017). Meanwhile, the accumulation of DIC may decrease porewater pH, potentially degrading the ecological environment.

In general, the degradation of organic carbon is considered the dominant process to add DIC to sediment porewater in coastal seas (Berner, 1980; Middelburg, 2018). Some studies have demonstrated that carbonate dissolution can be triggered by microbial respiration even in the calcite-oversaturated waters (Cai et al., 2006; Wang et al., 2025). The role of calcium carbonate ($CaCO_3$) dissolution in absorbing CO_2 and increasing total alkalinity (TA) in marine systems is recognized (Jahnke et al., 1997; Morse et al., 2006). Marine calcifying organisms are widely distributed throughout the ocean so surface sediments above the saturation horizon generally contain abundant $CaCO_3$ debris (Harikrishnan and Nathan, 2023; Ying et al., 2024), implying that both $CaCO_3$ dissolution and organic matter degradation likely occur ubiquitously within sediments. Some chamber experiments have demonstrated that the CO_2 produced from organic matter degradation drove $CaCO_3$ dissolution in marginal sea sediments. However, the extent of such CO_2-induced dissolution varied widely in different regions. As the chamber experiments mostly focus on biochemical influences on $CaCO_3$ dissolution, the constraints of dynamic processes are still unclear (Jahnke et al., 1994; 1997; Ortega et al., 2005). Moreover, the TA increased by $CaCO_3$ dissolution is demonstrated to mitigate the risks of water acidification induced by organic matter remineralization (Millero, 2007; Boudreau et al., 2018; LaRowe et al., 2020), but quantitative influence on the carbonate buffering capacity of seawater is also lack of constraint. Therefore, it is crucial to clarify the mechanism on biogeochemical cycling of inorganic carbon at the sediment-water interface, in particular when $CaCO_3$ dissolution may act as an important regulator maintaining the long-term stability of marine carbonate systems.

Sansha Bay in Fujian Province (China) represents one of major mariculture regions in the world and has undergone rapid expansion of seaweed farming in recent decades (FAO, 2024). Previous studies have

https://doi.org/10.5194/egusphere-2026-3442
Preprint. Discussion started: 29 June 2026

shown that the sediment carbon inventories under the farming zones have been ten times higher than those in non-mariculture seas (Duarte et al., 2025; Zhao, 2023; Wang et al., 2023). Despite such high productivity, the seawater in the bay does not deteriorate into acidification. In addition to active tidal exchange with shelf waters, $CaCO_3$ dissolution is hypothesized to play a key role in counteracting acidification (Wang et al., 2025). However, the regulating mechanism and quantitative influence on seawater are still unclear. In this study, a natural radionuclide approach (^{224}Ra–^{228}Th disequilibrium, Cai et al., 2015) was applied to quantify benthic fluxes of DIC and TA in Sansha Bay. By integrating stable carbon isotopic signatures ($\delta^{13}C$) of sedimentary carbon (Alling et al., 2012), we further identify the relative contributions of organic carbon degradation and $CaCO_3$ dissolution to benthic DIC release under different benthic environments, delineating the mechanism controlling sediment $CaCO_3$ dissolution. At last, the processes improving the seawater buffering capacity were recognized by comparing the changes of CO_2 and pH induced by various processes, elucidating the benthic influence on the carbonate system of seawater.

2 Materials and methods

2.1 Study sites and sample collection

Sansha Bay (26.5–26.8°N, 119.5–120.1°E) is a semi-enclosed bay located in southeastern China with water depths ranging from several meters to ~50 m. The local currents are dominated by tides and the rates of tidal currents are over 1 m s^{-1} near channel zones (Lin et al., 2019). The seaweed farms are widely distributed throughout Dongwuyang and the tidal zones adjacent to the main channels, and are controlled by regular semi-diurnal tides. Macroalgae-shellfish co-culture is the main practice of farms in Dongwuyang. The dominant macroalgae species are *Saccharina japonica* and *Gracilariopsis lemaneiformis*, and shellfish species are *Haliotis discus hannai* and *Crassostrea* (Wang et al., 2019).

Field work was conducted in 2024 and three stations were selected to represent contrasting mariculture settings (Fig. 1). Station SSW-A is located within the Dongwuyang seaweed farms, where the sediment contains abundant shell debris and polychaetes fragments (see Fig. S1 in Appendix). SSW-B is located in a sea cucumber culture zone adjacent to the main channel, with comparatively low farming intensity. SSW-C, near the bay mouth and outside the seaweed-farming zone, serves as a reference site for a non-mariculture condition. Water depth varied with tides and the specific depths during core collection ranged from 4–9 m. Detailed sampling information was listed in Appendix Table S1. In particular, sediments in the embayment are in great heterogeneity due to the mariculture behaviors. Human activities such as channel dredging and seasonal feeding can also change the sediment characters. The sampling sites in this study were mainly considered for the different hydrodynamic environments (inner and outer bay) and anthropogenic influences (with and without mariculture), not for the

https://doi.org/10.5194/egusphere-2026-3442
Preprint. Discussion started: 29 June 2026

100 representative of the whole embayment.

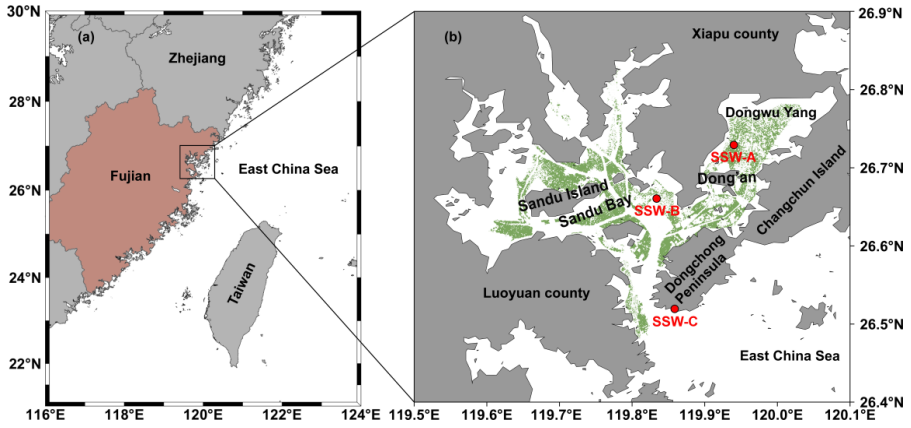

Figure 1: Sampling stations in Sansha Bay (red circles). The green-shaded area within the bay indicates the distribution of mariculture.

105

Bottom water was collected with a 5-liter Niskin bottle. Samples for carbonate parameters (DIC, TA and $\delta^{13}C_{DIC}$) were stored in 250 mL borosilicate glass bottles and ~5 L of water was transferred into a clean cubitainer for ^{224}Ra enrichment. Sediment cores were collected by a single-tube sampler, using polycarbonate tubes (i.d. 65 mm) with pre-drilled holes. After siphoning off the overlying water, sediment
110 porewater was extracted using Rhizon samplers via the holes at 1–2 cm intervals (Seeberg-Elverfeldt et al., 2005). Porewater from two cores was stored for carbonate analysis, ensuring the total volume >10 mL; the same depth porewater from different cores was combined so >30 mL porewater was used for a ^{224}Ra measurement. An intact core longer than 15 cm was sliced at a 1-cm interval for ^{224}Ra–^{228}Th disequilibria and particle analysis (Cai et al., 2015). The sediment was characterized by silty clay and
115 clayey silt. Seawater and porewater samples for DIC and TA were killed with saturated $HgCl_2$ solution by 0.5‰ (vol./vol.). Water samples for dissolved ^{224}Ra (D-^{224}Ra) were filtered through 142-mm glass fiber filters (GF/F) and stored at room temperature for radium enrichment.

2.2 Sample analysis

2.2.1 ^{224}Ra and ^{228}Th

120 Each of the sediment slices was transferred into a 250 mL Teflon beaker and mixed with approximately 200 mL of Milli-Q water. The slurry was thoroughly stirred and subjected to ultrasonication for 5–10 minutes to ensure complete dispersion of sediment particles. Subsequently, concentrated ammonia solution was added to the slurry to adjust the pH to 8–9. Thereafter 1.00 mL of

https://doi.org/10.5194/egusphere-2026-3442
Preprint. Discussion started: 29 June 2026

$KMnO_4$ solution (3.0 g L^{-1}) and 1.00 mL of $MnCl_2$ solution (8.0 g L^{-1} $MnCl_2 \cdot 4H_2O$) were sequentially added to form a MnO_2 suspension that coprecipitated Ra from the slurry. The particles of the slurry were filtered through a 142-mm GF/F filter (0.7-μm nominal pore size), and the bulk ^{224}Ra activity of the sediment was measured using a radium delayed coincidence counting system (RaDeCC, Scientific Instrument Inc., USA). After ~10 days and ~25 days, when ^{224}Ra had ingrown to secular equilibrium with its parent ^{228}Th, the second and third measurements were conducted in the same system. The final activities of both ^{224}Ra and ^{228}Th in the sediment were calculated from the first and the average of the last two measurements (Cai et al., 2012). A comparison between the last two runs was performed to check the reproducibility, yielding a mean ratio of 1.018 ± 0.026 (R^2 = 0.98, n = 29), suggesting that the RaDeCCs' efficiency kept stable during the analysis.

In the enrichment of D-^{224}Ra, 30–40 mL of porewater was transferred into a 100 mL Teflon beaker and ^{224}Ra was coprecipitated with MnO_2 following the similar procedure to the bulk ^{224}Ra. The precipitates were collected on a 47-mm GF/F filter. For the bottom water (~5 L), 5 mL of $KMnO_4$ (3.0 g L^{-1}) and $MnCl_2$ (8.0 g L^{-1} $MnCl_2 \cdot 4H_2O$) solutions were sequentially added into the sample and mixed for full reaction. The formed MnO_2 coprecipitates were then filtered onto a 142-mm GF/F filter. D-^{224}Ra activities were determined by counting the filters in RaDeCCs for more than 8 hours (Cai et al., 2015).

The final ^{224}Ra and ^{228}Th activities were corrected with chance coincidences, detector efficiencies and self-decay (Cai et al., 2012), and the uncertainties, propagated from counting statistics, were approximately 5% for total ^{224}Ra-^{228}Th and 8–10% for D-^{224}Ra. According to the standard deviation of the activity ratios of ^{224}Ra to ^{228}Th ($^{224}Ra/^{228}Th$) in aged sediment samples (n = 29), sediment layers with $^{224}Ra/^{228}Th$ of 1.00 ± 0.05 were considered to be in secular equilibrium between ^{224}Ra and ^{228}Th.

2.2.2 DIC, $\delta^{13}C_{DIC}$ and TA

The DIC concentrations in seawater and porewater were determined with a non-dispersive infrared analyzer (Li-Cor 7000, USA) after acidification with a mixture of 3% H_3PO_4 and 7% NaCl (Sun et al., 2024). The relative standard deviation (RSD) of replicates was well controlled less than 0.2%. The $\delta^{13}C_{DIC}$ (‰) was analyzed with an automatic DIC-$\delta^{13}C$ analyzer with an accuracy (1σ) of ±0.1‰ (Picarro G2131-i, USA). The TA was measured following the Gran titration (Gran, 1952). Porewater samples were first diluted with TA-known aged seawater. The titrant was 0.1 mol L^{-1} HCl and the titration was automatically terminated using a titrator (Apollo AS-ALK3, USA) with an Orion AR1-17304 pH electrode. Each TA sample was measured 2–3 times, yielding the RSD within ±0.5% after volume correction. Both DIC and TA concentrations were calibrated with Scripps Certified Reference Material (CRM, Batch #198) (Dickson et al., 2003).

https://doi.org/10.5194/egusphere-2026-3442
Preprint. Discussion started: 29 June 2026

2.2.3 The $\delta^{13}C$ isotope of sediment TOC ($\delta^{13}C_{TOC}$)

Dried sediment samples were ground and homogenized with a mortar and pestle. Approximate 1 g of each sample was weighed and acidified with 1.2 N HCl (guaranteed reagent, GR). The mixture was subjected to ultrasonication for 1 h, followed by a 5-h water bath at 60°C to completely remove the inorganic carbon. Subsequently, the samples were repeatedly rinsed with Milli-Q water until the pH of the supernatant was neutral. The remaining particles were then dried at 60°C and accurately weighed. The mass loss relative to the dry sediment was assumed as total $CaCO_3$ in this study. Total inorganic carbon (TIC) was calculated from $CaCO_3$ and the precision (0.1 mg) was based on that of the weight scale. The TOC content was determined using an elemental analyzer (vario ISOTOPE, Elementar., Germany) and calibrated with an acetanilide standard (Sigma-Aldrich). The $\delta^{13}C_{TOC}$ was simultaneously measured with a continuous-flow isotope ratio mass spectrometer and the accuracy (1σ) was ±0.1‰.

2.3 Benthic effluxes estimated from ^{224}Ra–^{228}Th disequilibria

In Sansha Bay, intensive aquaculture activities introduce shell fragments and coarse particles into the sediments (see Appendix Fig. S1). Influenced by tidal currents and biological activities, the sediment in the bay is generally permeable. The exchangeable interface between sediment and seawater is further extended by active benthic faunal irrigation. In such a dynamic system, traditional methods such as diffusion or incubation experiments may fail to accurately estimate benthic exchange fluxes (Shi et al., 2018). In contrast, the ^{224}Ra–^{228}Th disequilibrium approach has been confirmed as a robust method for capturing complex interfacial processes in most China coastal seas (Shi et al., 2019).

In the ^{232}Th decay series, ^{224}Ra is the daughter of ^{228}Th. Owing to the distinct particle reactivities, ^{224}Ra can be desorbed from particles in saline waters, whereas ^{228}Th remains strongly bound on sediment particles. With exchanges between bottom waters and porewaters, total ^{224}Ra generally presents deficits relative to its parent ^{228}Th in surface sediments (Cai et al., 2015). Therefore, the ^{224}Ra efflux (F_{Ra}) across the sediment-water interface can be quantified from the disequilibria between ^{224}Ra and ^{228}Th (Eq. 1, Cai et al., 2015):

$$F_{Ra} = \lambda_{Ra} \int_0^z (A_{Th} - A_{Ra})dz \quad (1)$$

where λ_{Ra} represents the decay constant of ^{224}Ra (0.189 d^{-1}), A_{Ra} and A_{Th} represent the ^{224}Ra and ^{228}Th activities in bulk sediments (dpm cm^{-3}) corrected with porosity (Φ), respectively, and z denotes the depth at which ^{224}Ra and ^{228}Th approach secular equilibrium. This efflux reflects the synergistic effect with molecular diffusion, bioturbation and irrigation at the interface so a diffusion model embedding increased surface area can be applied to stand for the exchange:

$$F_{Ra} = \xi \Phi D_s^{Ra} \frac{\partial A_{DRa}}{\partial z} \quad (2)$$

where ξ denotes the factor indicating the enhancement of exchangeable area, D_s^{Ra} represents the

https://doi.org/10.5194/egusphere-2026-3442
Preprint. Discussion started: 29 June 2026

molecular diffusion coefficient of ^{224}Ra that has been corrected with in-situ temperature and sediment porosity, and $\frac{\partial A_{DRa}}{\partial z}$ is the ^{224}Ra activity gradient at the sediment-water interface.

Under the same circumstance, the area-enhancement model should be appropriate to other solutes so the benthic fluxes of carbonate parameters (DIC and TA) can be estimated as

$$F_m = \xi \Phi D_s^m \frac{\partial C^m}{\partial z} \quad (3)$$

where F_m refers to the benthic flux of DIC or TA across the sediment-water interface, D_s^m represents the diffusion coefficient of bicarbonate (HCO_3^-), and $\frac{\partial C^m}{\partial z}$ denotes the concentration gradient of DIC or TA at the interface.

2.4 The model for tracing sources of porewater DIC

In marine environments, $\delta^{13}C_{TOC}$ is generally around -20‰ (Jahnke et al., 1997; Hu and Burdige, 2007), whereas $CaCO_3$ in shells exhibits $\delta^{13}C$ values ($\delta^{13}C_{CaCO_3}$) ranging from -7.7‰ to -2.6‰ (Surge et al., 2001; Gillikin et al., 2006; Hadden et al., 2018). Although sediment porewater is derived from bottom seawater, the degradation of organic matter and the dissolution of $CaCO_3$ in sediments can add lighter carbon to porewater DIC (DIC_{PW}), resulting in the $\delta^{13}C$ of DIC_{PW} more negative than those of bottom water (DIC_{BW}). Assuming that the differences in DIC concentrations between bottom water and porewater are solely attributed to the two processes (organic carbon degradation and $CaCO_3$ dissolution), their relative contributions to the porewater DIC can be defined as f_{TOC} and f_{CaCO_3}, namely

$$f_{CaCO_3} + f_{TOC} = \frac{DIC_{PW} - DIC_{BW}}{DIC_{PW}} \quad (4)$$

The isotopic composition of DIC in porewater ($\delta^{13}C_{PW}$) can be expressed as (Alling et al., 2012)

$$\delta^{13}C_{PW} \cdot DIC_{PW} = \delta^{13}C_{BW} \cdot DIC_{BW} + \delta^{13}C_{CaCO_3} \cdot f_{CaCO_3} \cdot DIC_{PW} + \delta^{13}C_{TOC} \cdot f_{TOC} \cdot DIC_{PW} \quad (5)$$

where $\delta^{13}C_{BW}$ represents the $\delta^{13}C$-DIC in bottom water; and $\delta^{13}C_{CaCO_3}$ and $\delta^{13}C_{TOC}$ stand for the $\delta^{13}C$ of shell debris and organic carbon (TOC) in the sediment, respectively. By combining Eq. (4) and Eq. (5), f_{TOC} and f_{CaCO_3} can be calculated.

2.5 Significance Tests

Significance tests were performed using R (R Core Team, 2023). The Shapiro–Wilk test (shapiro.test) was used to assess the normality of $\delta^{13}C_{DIC}$ in porewaters and bottom waters, and a *t*-test was applied for the value comparison. In Sect. 4.3, a linear mixed-effects model (from the package 'lme4') was employed to test whether the theoretical $\delta^{13}C_{DIC}$ derived solely from TOC degradation matched the measured porewater $\delta^{13}C_{DIC}$.

https://doi.org/10.5194/egusphere-2026-3442
Preprint. Discussion started: 29 June 2026

3 Results

3.1 The distributions of ^{224}Ra and ^{228}Th in the sediment

The total ^{224}Ra and ^{228}Th present similar vertical distributions in sediments as ^{224}Ra is derived from the radioactive decay of ^{228}Th (Fig. 2a). At SSW-A and SSW-C, deficits of ^{224}Ra, with the average ^{224}Ra/^{228}Th of 0.89 ± 0.05 (n = 14, 1SD), were observed in the upper 10 cm, whereas equilibrium between ^{224}Ra and ^{228}Th was characterized below 12 cm (^{224}Ra/^{228}Th = 0.98 ± 0.03, n = 4). For SSW-B, the total ^{224}Ra was nearly in equilibrium with ^{228}Th (Fig. 2b). In the outer-bay sediments (SSW-C), the ^{224}Ra and ^{228}Th activities were in the range of 1.70 ± 0.10–4.55 ± 0.29 dpm g^{-1} and 2.01 ± 0.06–4.54 ± 0.16 dpm g^{-1}, respectively. In comparison, the sediment in the inner bay (SSW-A and SSW-B) had lower radionuclide activities (1.34 ± 0.09–3.00 ± 0.20 dpm g^{-1} for ^{224}Ra and 1.40 ± 0.0 5–3.25 ± 0.10 dpm g^{-1} for ^{228}Th, Table S1 in Appendix).

Vertical profiles of D-^{224}Ra activities in porewater and bottom water (depth = 0) are presented in Fig. 2c. The activities of D-^{224}Ra in bottom water, ranging from 0.11 ± 0.01 to 0.39 ± 0.02 dpm L^{-1}, were 1–2 orders of magnitude lower than those in porewaters (Table S2 in Appendix). The differences in porewater D-^{224}Ra between stations were consistent with the total ^{224}Ra in sediments. Namely, D-^{224}Ra activities at SSW-C (16.2 ± 1.9–52.4 ± 3.1 dpm L^{-1}) were higher than those at inner-bay stations (4.0 ± 0.8–25.8 ± 2.4 dpm L^{-1}). At depths where total ^{224}Ra was deficient relative to ^{228}Th, D-^{224}Ra activities exhibited obvious variations. Correspondingly, layers where ^{224}Ra–^{228}Th activities approached equilibria, such as 4-10 cm at SSW-B, coincided with stable distributions of D-^{224}Ra (RSD < 7%).

https://doi.org/10.5194/egusphere-2026-3442
Preprint. Discussion started: 29 June 2026

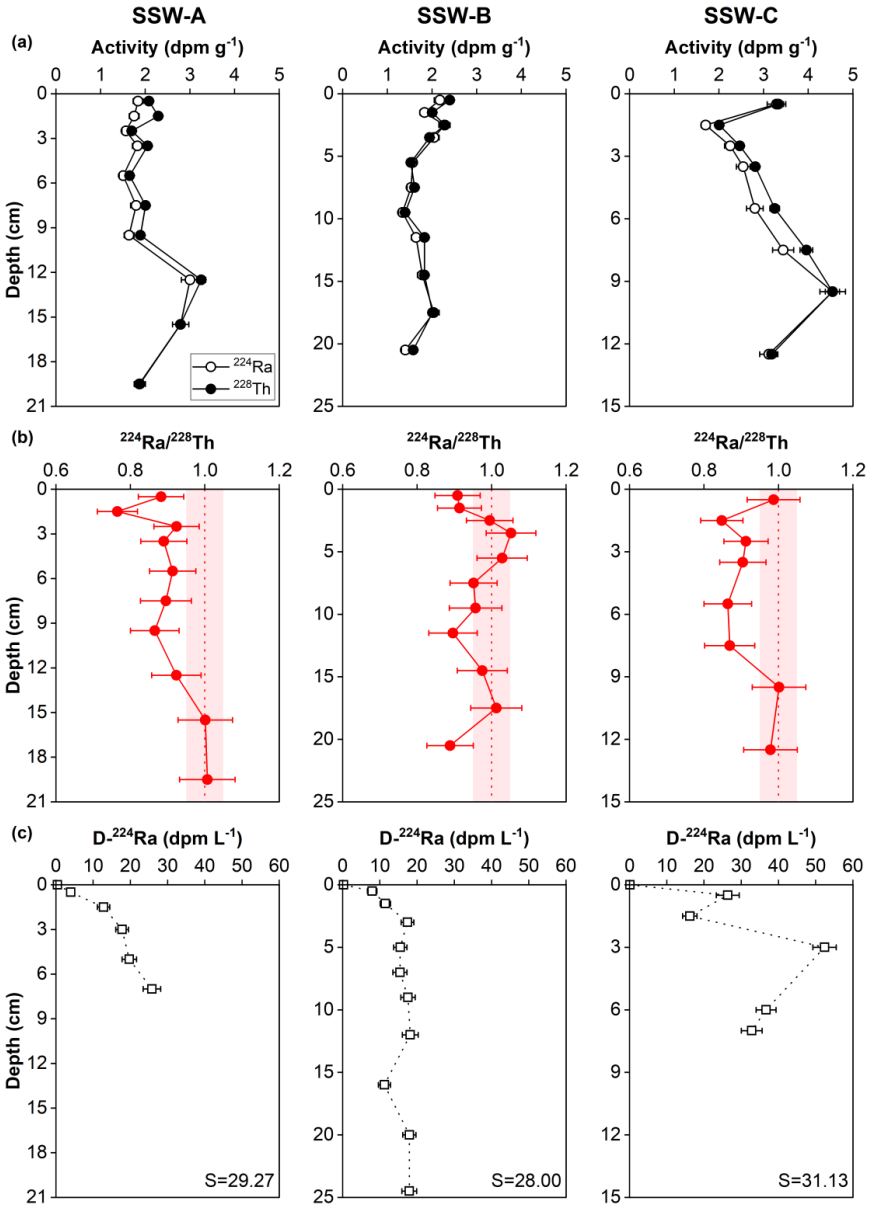

Figure 2: (a) Vertical profiles of bulk ^{224}Ra and ^{228}Th (error = ± 1σ) activities in the sediment. (b) Activity ratios of ^{224}Ra to ^{228}Th, with the shaded indicating secular equilibrium between ^{224}Ra and ^{228}Th (^{224}Ra/^{228}Th = 1.0 ± 0.05); (c) Vertical profiles of D-^{224}Ra (error = ± 1σ) in porewater (the symbol at depth = 0 represents the bottom water). Note that the activity ranges and depth ranges differ slightly among stations.

https://doi.org/10.5194/egusphere-2026-3442
Preprint. Discussion started: 29 June 2026

3.2 The distributions of DIC, TA, and $\delta^{13}C_{DIC}$ in the porewater

In the bottom water, the DIC and TA concentrations were in the range of 1964–2229 μmol kg^{-1} and 1982–2357 μmol kg^{-1}, respectively. The porewater exhibited particularly higher DIC and TA (ranging from 2184 to 3007 μmol kg^{-1}, from 2326 to 3081 μmol kg^{-1}, respectively) than the bottom water (Table S3 in Appendix). At SSW-A and SSW-C, the DIC and TA concentrations generally increased with depth (Fig. 3). At SSW-B, unexpectedly, both DIC and TA concentrations decreased with depth below 3 cm, and the concentrations of DIC above 15 cm were higher than TA.

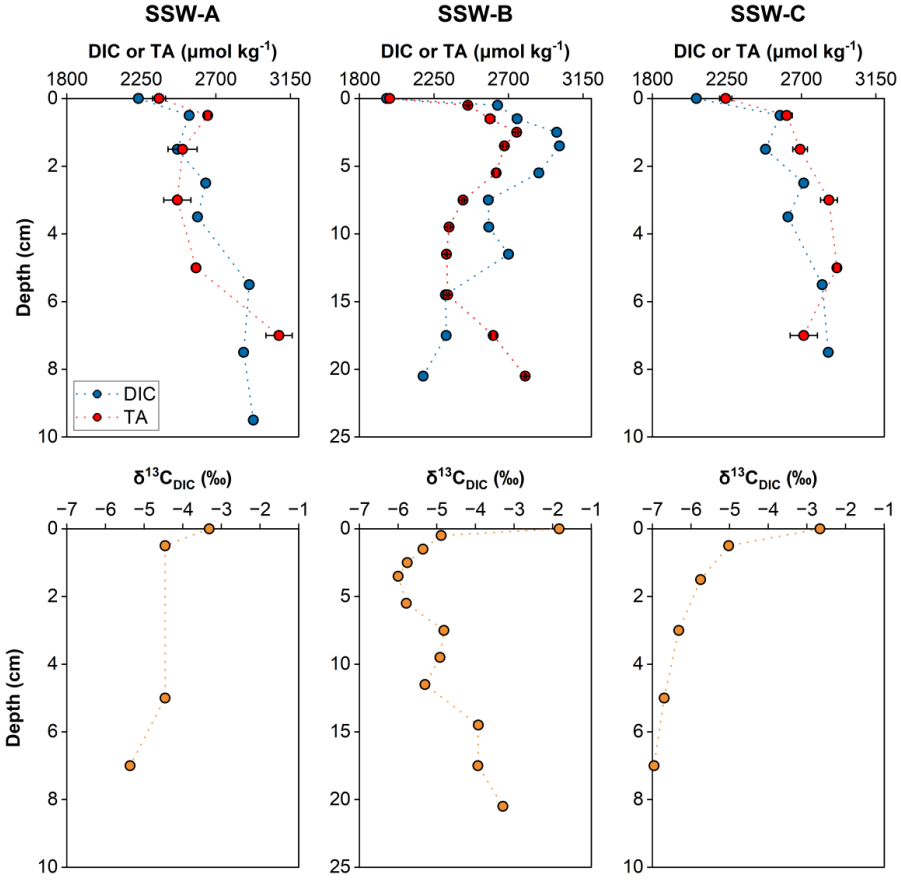

Figure 3: Vertical profiles of DIC, TA (error = ± 1SD), and $\delta^{13}C_{DIC}$ in porewater, where depth = 0 represents the bottom water layer. Note that the depth ranges at Station SSW-B are different from the other stations.

In comparison, the profiles of porewater $\delta^{13}C_{DIC}$ and DIC overall exhibited opposite trends although

https://doi.org/10.5194/egusphere-2026-3442
Preprint. Discussion started: 29 June 2026

the $\delta^{13}C_{DIC}$ values at station SSW-A were discrete due to the restricted number of samples (Fig. 3). The $\delta^{13}C_{DIC}$ of the bottom water in our study area ranged from -3.3‰ to -1.8‰, more negative than the values of offshore waters in the East China Sea (-2.0–0.5‰) (Wang et al., 2016; Duan et al., 2022). The $\delta^{13}C_{DIC}$ values of the porewater varied between -7.0‰ and -3.3‰, significantly lower than those of the bottom water ($p < 0.001$, *t*-test, Fig. 4). Especially, the porewater $\delta^{13}C_{DIC}$ at SSW-A was the heaviest while that at SSW-C contained the lightest $\delta^{13}C_{DIC}$ although the DIC concentrations of the two stations were comparable.

3.3 The $\delta^{13}C$ in shells and sediment TOC

Shells for $\delta^{13}C_{CaCO_3}$ were collected from oysters and abalones and the values ranged from -4.5‰ to -3.4‰ (n = 9) with a median of -3.8‰ (Fig. 4). The sediment $\delta^{13}C_{TOC}$ of all subsamples was in the range of -24.6– -22.4‰ (n = 27), the median of which was -23.3‰. In particular, the TIC contents were highest in the sediment of SSW-A (15.4 to 35.4 mg g^{-1}, Table S1 in Appendix), coincident with the abundant shell debris in the sediment and the relatively positive porewater $\delta^{13}C_{DIC}$ at this station (Fig. S1 in Appendix).

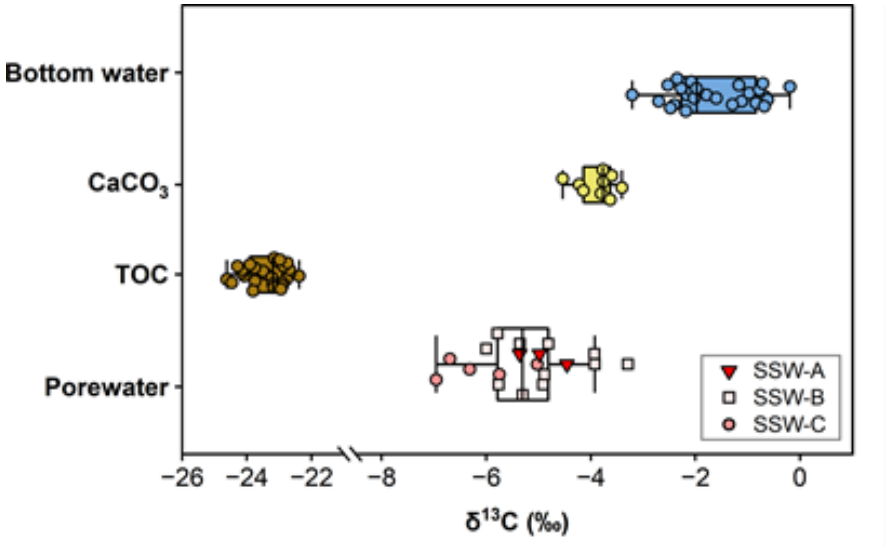

Figure 4: The $\delta^{13}C$ values in different matrix. $CaCO_3$ represents shells collected from oysters and abalones. TOC refers to the sediment TOC at our sampling sites.

https://doi.org/10.5194/egusphere-2026-3442
Preprint. Discussion started: 29 June 2026

4 Discussion

4.1 The mechanism of interfacial exchange revealed by the ^{224}Ra–^{228}Th disequilibria

In comparison of ^{224}Ra profiles, the high D-^{224}Ra in porewater corresponds to the high bulk ^{224}Ra in sediment (SSW-C). The layers where ^{224}Ra–^{228}Th activities presented disequilibria coincided with great variations of D-^{224}Ra (RSD of three adjacent D-^{224}Ra larger than 10%), indicating that the sediment served as the major source of D-^{224}Ra. As the ^{224}Ra–^{228}Th disequilibria provided a reliable indicator of D-^{224}Ra transfer, the ^{224}Ra effluxes (F_{Ra}), as well as the interface area factor (ξ), were calculated with the method in Sect. 2.3 (Eq. 1 and Eq. 2) based on the activity gradients of D-^{224}Ra at the sediment-water interface (Table 1). The integration depth of SSW-A and SSW-C was set at the first layer where the ^{224}Ra and ^{228}Th reached equilibrium. For SSW-B, the full core was integrated as the radionuclides were basically in equilibrium. The gradients were calculated from the D-^{224}Ra activity differences between 0-1 cm porewater and bottom water.

Although the ^{224}Ra fluxes at SSW-A and SSW-C were similar, the ξ at SSW-A was 6–7 times higher. Given that SSW-A was located in seaweed farms where dense macrobenthic communities existed (Wang et al., 2019), the sediment contained abundant burrows and tunnels generated by benthic fauna activities, effectively increasing the area of the sediment-water interface and thereby enhancing the ^{224}Ra flux. In contrast, the ξ values at SSW-B and SSW-C were comparable but the ^{224}Ra flux at SSW-C was approximately three times higher, implying that processes other than bioturbation stimulated the benthic exchange at SSW-C. As the Dongchong Channel is dominantly affected by semi-diurnal tides, the sediment-water interface at SSW-C nearby is subject to stronger hydrodynamics than SSW-B (Lin et al., 2017). Fine particles were entrained to open waters by tidal currents and the coarser ones were retained so the sediment at SSW-C was of permeability. Therefore, the benthic effluxes were dominated by bioactivities in inner-bay mariculture zones while tidal currents and flow turbulence accounted for the active interfacial exchange in outer-bay zones.

https://doi.org/10.5194/egusphere-2026-3442
Preprint. Discussion started: 29 June 2026

Table 1: The molecular diffusion coefficient of ^{224}Ra (D_s^{Ra}), the activity gradient of D-^{224}Ra ($\frac{\partial A^{Ra}}{\partial z}$), the integration depth (z_{int}) used to calculate the benthic flux of ^{224}Ra, the ^{224}Ra flux (F_{Ra}) and the interface area enhancement factor (ξ) at each sampling station. Uncertainties for all parameters are reported as ± 1σ.

Station	D_s^{Ra} (10^{-6} cm^2 s^{-1})	$\frac{\partial A^{Ra}}{\partial z}$ (dpm L^{-1} cm^{-1})	z_{int} (cm)	F_{Ra} (dpm cm^{-2} d^{-1})	ξ
SSWA	4.5	7.16 ± 1.54	16	0.53 ± 0.11	260.1 ± 78.44
SSWB	4.4	15.4 ± 2.50	21	0.17 ± 0.08	41.22 ± 19.49
SSWC	3.8	52.5 ± 6.15	10	0.54 ± 0.13	44.75 ± 11.64

Moreover, the ^{224}Ra effluxes were utilized to quantify the residence time (τ) of the bay water if we assumed that the addition of ^{224}Ra in the inner bay were all derived from the sediment. According to the ^{224}Ra activities of water column in Sansha Bay (Wang et al., 2018), we constrained the endmembers in Sandu Bay and selected the ^{224}Ra activities of mid-salinity tidal water and bay-mouth seawaters to plot the conservative mixing line (Fig. S2a in Appendix). Consequently, low-salinity inputs from rivers or submarine groundwater discharge were not included in this model. Excess ^{224}Ra above the conservative line (ΔRa) was assumed to be derived from the sediment so τ can be estimated as

$$\tau = \frac{\Delta Ra}{F_{Ra}} h \quad (6)$$

where h denotes the average water depth of the bay, and a value of 14 ± 3 m was assigned in consideration of the tidal ranges and the water depths measured during the field work. Since all of seawater ^{224}Ra referred to were collected within Sandu Bay (Wang et al., 2018; Fig. S2b in Appendix), we adopted the ^{224}Ra flux of SSW-B, which is located in the middle of the bay, to represent the average benthic ^{224}Ra input to the bay (F_{Ra}). It should be noted that the ^{224}Ra released from the sediment was assumed to be rapidly mixed into seawater due to the influence of semi-diurnal tides, and that the radioactive decay of ^{224}Ra was not considered due to the frequent water exchange in this model. Therefore, the τ estimated here represents the low limit of the water residence time. By substituting these values into Eq. (6), the seawater residence time based on ΔRa of Sandu Bay ranged from 0.11 to 3.7 days (Fig. S2b), comparable to those of the wet season (0.2–3.0 days) in Sandu Bay estimated by the seawater $^{224}Ra/^{228}Ra$ (Wang et al., 2018).

4.2 Fluxes of DIC and TA across the sediment-water interface

By applying the area-enhancement model to other solutes (Eq. 3 in Sect. 2.3), the benthic fluxes of

https://doi.org/10.5194/egusphere-2026-3442
Preprint. Discussion started: 29 June 2026

DIC and TA at each station were estimated. The gradients of DIC and TA were calculated from the concentration differences between 0-1 cm porewater and bottom water (Table 2). The largest DIC and TA fluxes, approximately 600 mmol m^{-2} d^{-1}, were exhibited in the farming zone (SSW-A) although the porewater DIC and TA concentrations were not the highest. The fluxes at the other two stations ranged from 105 to 207 mmol m^{-2} d^{-1}. The magnitude of these DIC fluxes is comparable to the estimates in the intermediate-salinity zones of the nearby Jiulong River estuary (26–1000 mmol m^{-2} d^{-1}, Hong et al., 2017). In particular, the high benthic DIC and TA fluxes were dominated by the enlarged interface areas (ξ). If only molecular diffusion was considered, benthic DIC flux at SSW-A (~2.4 mmol m^{-2} d^{-1}) fell within the reported range derived from the porewater gradient model (0.54–2.65 mmol m^{-2} d^{-1}, Jahnke et al.,1997), a method that has been confirmed to underestimate benthic exchanges (Glud et al., 2016). The decoupling between fluxes and concentration gradients (Table 2) indicates that dynamic processes are important in interfacial exchanges and must therefore be involved in the quantification of benthic effluxes.

Ortega et al. (2005) compiled DIC and TA fluxes measured using benthic chambers, reporting ranges of 5–700 mmol m^{-2} d^{-1} and 1–200 mmol m^{-2} d^{-1}, respectively. The relatively low fluxes were attributed to the exclusion of advective transport by chambers. In their studies of three Cantabrian estuaries, despite in-situ flow rates differing by an order of magnitude, the average of benthic DIC effluxes, 342, 252 and 217 mmol m^{-2} d^{-1}, were similar. Although the porewater DIC and TA in Sansha Bay were not particularly high, the fast currents in the bay (~1 m s^{-1}; Lin et al., 2017) strengthened the benthic exchange by irrigating the permeable sediment. Consequently, the DIC effluxes at stations SSW-B and -C were comparable to the chamber results in Cantabrian estuaries, where organic carbon oxidation was considerable. Furthermore, the current influence was amplified when the sediment was also subject to intensive benthos disturbance. As a result, the DIC and TA fluxes in the farming zone (SSW-A) were higher by a factor of 3–5 than others.

To illustrate the benthic influence on water columns, we used modified Eq. (6) to estimate the increased DIC and TA derived from the sediment (ΔDIC_{sw} and ΔTA_{sw}). Here the residence time (τ) from Sandu Bay were adopted owing to the similar hydrodynamic conditions (Table 2). As a result, the benthic release at SSW-A contributed the largest amounts of DIC and TA to the water column (>150 μmol kg^{-1}, Table 2). In the meantime, elevated DIC and TA concentrations were observed in Dongwuyang, where the average concentrations of DIC and TA were higher by 122 μmol kg^{-1} and 64 μmol kg^{-1} than those in the main channel, respectively (Fig. S3 in Appendix). The elevations were consistent with the magnitudes of ΔDIC_{sw} and ΔTA_{sw}, confirming that the sediment served as the dominant source of DIC and TA in the inner bay. In contrast, stations close to channels showed minimal sediment influences on seawater concentrations (< 15 μmol kg^{-1}), indicating that tidal exchange was the dominant factor for the variations of DIC and TA in the outer bay. This corresponds to the dynamic mechanism regulating the interfacial exchange at SSW-C illustrated by the ^{224}Ra–^{228}Th disequilibria. However, we need to point out that the

https://doi.org/10.5194/egusphere-2026-3442
Preprint. Discussion started: 29 June 2026

estimates here only reflect an average efflux over two weeks around sampling time as the time scale of the ^{224}Ra-^{228}Th disequilibrium approach is constrained by the half-life of ^{224}Ra (3.66 days). Given that there are great spatial and temporal heterogeneity on sediments in Sansha Bay, these effluxes are not suitable for assessments of annual exchange or carbon budget of the whole bay.

Table 2: The summary of parameters for flux calculation including the molecular diffusion coefficients of DIC (D_s^{DIC}) and the concentration gradients of DIC and TA at the interface ($\frac{\partial C^m}{\partial z}$), and benthic flux of DIC and TA (F_m) at each sampling station. The last three rows represent the residence time (τ) and increased concentrations of DIC and TA to the water column (ΔDIC_{sw} and ΔTA_{sw}) estimated from Fm and τ. Uncertainties for all parameters are reported as ± 1σ.

Parameters \ Stations	SSW-A	SSW-B	SSW-C
*D_s^{DIC} (10^{-6} cm^2 s^{-1})	6.0	5.9	5.1
$\frac{\partial C^{DIC}}{\partial z}$ (μmol L^{-1} cm^{-1})	626.5	1367	1033
$\frac{\partial C^{TA}}{\partial z}$ (μmol L^{-1} cm^{-1})	598.2	963.7	754.8
F_{DIC} (mmol m^{-2} d^{-1})	624 ± 188	207 ± 97.4	143 ± 37.3
F_{TA} (mmol m^{-2} d^{-1})	595 ± 180	146 ± 68.7	105 ± 27.3
F_{TA}/F_{DIC}	0.95 ± 0.40	0.70 ± 0.47	0.73 ± 0.27
τ (d)	3.73 ± 0.38	0.86 ± 0.09	0.24 ± 0.03
ΔDIC_{sw} (μmol kg^{-1})	163 ± 62.5	12.6 ± 6.7	2.4 ± 0.9
ΔTA_{sw} (μmol kg^{-1})	156 ± 59.6	8.9 ± 4.7	1.8 ± 0.6

* The dominant component of DIC and TA is HCO_3^- so the same diffusion coefficient is used.

In a semi-enclosed embayment, Luoyuan Bay, located close to our study region, the settling fluxes of particulate organic carbon (POC) estimated using sediment traps were reported to range from 92 to 375 mmol C m^{-2} d^{-1}, comparable with those on the inner shelf of the East China Sea (60–608 mmol C m^{-2} d^{-1}) (Hung et al., 2013; Wang et al., 2018). As the sediment trap was deployed in a shallow aquaculture zone during a macroalgae blooming, we supposed that Sansha Bay exhibited a similar range of POC flux. Correspondingly, the DIC released from sediment were equal or even higher than the deposited POC. This indicates, on one hand, that the sediment was characterized with intense microbial activities, allowing rapid remineralization of the deposited POC. Furthermore, the higher DIC efflux relative to POC

https://doi.org/10.5194/egusphere-2026-3442
Preprint. Discussion started: 29 June 2026

flux suggests that organic carbon degradation was not the sole process responsible for DIC increment in the sediment, particularly in the inner bay (SSW-A).

4.3 The contributions of organic carbon degradation and $CaCO_3$ dissolution to porewater DIC

With the method in Sect. 2.4, conservative DIC addition to porewater relative to the bottom water and porewater $\delta^{13}C_{DIC}$ variations were used to quantify the contributions of organic carbon degradation and $CaCO_3$ dissolution. The medians of $\delta^{13}C$ in shells and sediment TOC were selected to represent the characteristics of the processes that added DIC to porewaters, namely $\delta^{13}C_{CaCO_3}$ = -3.77‰ and $\delta^{13}C_{TOC}$ = -23.19‰ (Fig. 4). In order to prove the necessity of including $CaCO_3$ dissolution, TOC degradation as a sole DIC addition was modelled with the modified Eq. (5), $\delta^{13}C_{PW} = \delta^{13}C_{BW}\frac{DIC_{BW}}{DIC_{PW}} + \delta^{13}C_{TOC}\frac{DIC_{PW} - DIC_{BW}}{DIC_{PW}}$). The theoretical porewater $\delta^{13}C_{DIC}$ as a result of TOC degradation only would range from -9.2‰ to -4.0‰ (red plots in Fig. 5, data in Table S3), significantly different from the measured $\delta^{13}C_{DIC}$ in the porewater ($p < 0.001$, Liner mixed-effects model; blue plots in Fig. 5). The negative deviation indicates that other source with heavier carbon than TOC, i.e., $CaCO_3$, collectively influenced the porewater DIC concentrations.

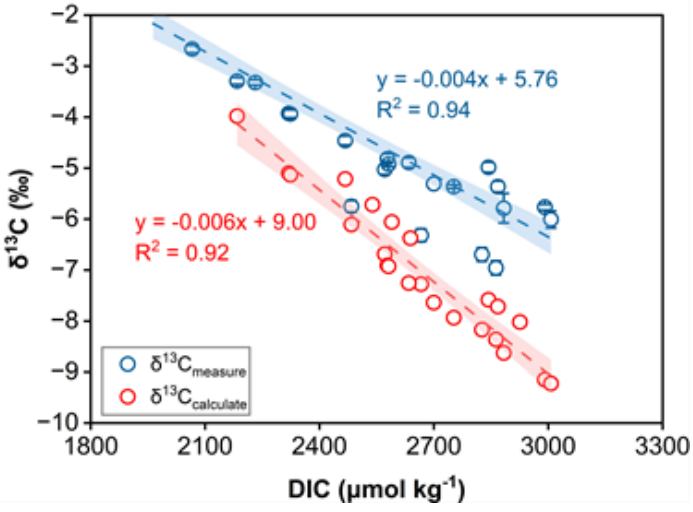

Figure 5: The correlations between $\delta^{13}C$ and DIC concentrations, where $\delta^{13}C_{measure}$ (error = ± 1σ) represents the laboratory-measured porewater $\delta^{13}C_{DIC}$, and $\delta^{13}C_{calculate}$ represents the theoretical $\delta^{13}C_{DIC}$ values influenced solely by organic carbon degradation. The shaded areas represent the 95% confidence intervals.

https://doi.org/10.5194/egusphere-2026-3442
Preprint. Discussion started: 29 June 2026

According to the original Eq. (5), the contributions of TOC degradation (f_{TOC}) and $CaCO_3$ dissolution (f_{CaCO_3}) were quantified (Table S4 in Appendix). Overall, bottom water dominated the composition of porewater. The TOC degradation contributed 5.6–20.5% of the porewater DIC and f_{CaCO_3} were in the range of 1.8–17.5% while the relative contributions between f_{TOC} and f_{CaCO_3} varied between stations (Fig. 6). It is evident that $CaCO_3$ dissolution played a greater role than TOC degradation at SSW-A, consistent with the phenomenon of abundant shell debris and the highest TIC content in the sediment (Table S1 in Appendix). At SSW-B where sea cucumber mariculture existed, f_{TOC} was elevated and the DIC concentrations of the porewater were also higher than others. This enhancement is likely associated with the decomposition of organic matters accumulated from local feeding. In contrast, f_{TOC} was significantly higher than f_{CaCO_3} at SSW-C ($p < 0.005$, *t*-test) where TIC content was relatively low. It seems that high degradation of organic carbon cannot always lead to a high $CaCO_3$ dissolution, suggesting that except for the sediment matrix, the bottom hydrodynamics may influence the relative proportions. As SSW-C was located near the bay mouth and the water exchange was active, the oxic environment promoted the organic matter degradation in the surface sediment. But the strong interfacial exchange limited the CO_2 accumulation, consequently weakening the $CaCO_3$ dissolution in the sediment. By comparison, the DIC was enriched in the sediment porewater at the inner-bay stations so more $CaCO_3$ dissolution was triggered. The inference is also supported by the vertical variation of SSW-B: the highest f_{CaCO_3} and f_{TOC} were presented in the subsurface sediment where DIC was highest; and meanwhile, the lowering f_{CaCO_3} with depth showed the opposite effect that $CaCO_3$ dissolution was weakened when the porewater DIC was diluted as a result of seawater irrigation.

https://doi.org/10.5194/egusphere-2026-3442
Preprint. Discussion started: 29 June 2026

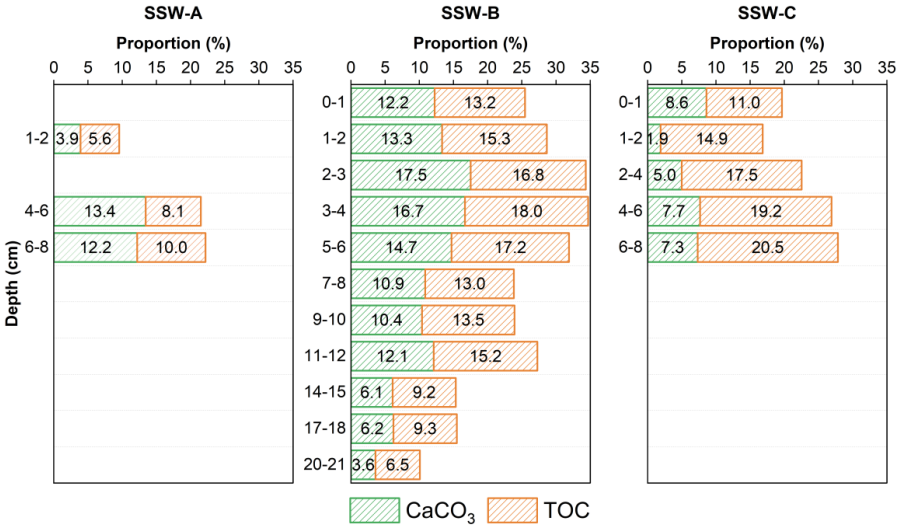

Figure 6: The contribution proportions of organic carbon degradation (f_{TOC}, orange bars) and $CaCO_3$ dissolution (f_{CaCO_3}, green bars) to porewater DIC in different sediment layers. Values within bars indicate the respective proportion.

The average ratios between f_{CaCO_3} and f_{TOC} (f_{CaCO_3}/f_{TOC}) of SSW-A, SSW-B and SSW-C were 1.2, 0.8 and 0.4, respectively (Table S4). Hence, the DIC efflux contributed by $CaCO_3$ dissolution at each station was estimated to be 339 ± 102, 92.7 ± 43.6 and 40.2 ± 10.4 mmol m^{-2} d^{-1}, respectively ($F_{CaCO_3} = F_{DIC} \frac{1}{1+\frac{f_{TOC}}{f_{CaCO_3}}}$), contributing 27–56% of the total DIC efflux. These ratios are in agreement with the results of previous studies that about one third to half of DIC fluxes were derived from $CaCO_3$ dissolution in benthic chambers (Ortega et al., 2005; Jahnke et al., 1997). The chamber studies well demonstrated that the CO_2 produced by aerobic and anaerobic degradation was vital for $CaCO_3$ dissolution in sediments and supported the trigger mechanism in this study. Furthermore, we introduced the hydrodynamic conditions in explaining the different extents of $CaCO_3$ dissolution that were hardly simulated in past research: except for the metabolic CO_2, the intensity of interfacial exchange determined whether the CO_2 could be accumulated to produce a microenvironment for continuous dissolution. This study provides a new perspective on the reason why the role of metabolic CO_2 in $CaCO_3$ dissolution varied regionally in previous studies.

4.4 Sediment influence on the carbonate buffering capacity of seawater

As the sources of porewater DIC have been illustrated in Sect. 4.3, the same ratios f_{CaCO_3}/f_{TOC} (1.2, 0.8 and 0.4 for SSW-A/B/C) were applied to reflect the benthic influence on the seawater. Based on the

https://doi.org/10.5194/egusphere-2026-3442
Preprint. Discussion started: 29 June 2026

benthic addition to the water column estimated in Sect. 4.2, the seawater DIC and TA without sediment influence (DIC_0 and TA_0) can be calculated by deducting ΔDIC_{sw} and ΔTA_{sw} from the measured DIC and TA of seawater (Table 2). Similar with the efflux contributions, the changes of DIC concentrations in seawater that was attributed to organic matter degradation (ΔDIC_{TOC}) was estimated as 71.5, 7.9 and 1.8 μmol kg^{-1} for SSW-A, SSW-B and SSW-C, respectively ($\Delta DIC_{TOC} = \Delta DIC_{sw} \frac{1}{1+\frac{f_{CaCO_3}}{f_{TOC}}}$). If there was only aerobic mineralization occurring in the sediment, the DIC in seawater would be $DIC_0 + \Delta DIC_{TOC}$ while the change of TA was assumed to be negligible. The DIC and TA concentrations we measured in seawater are reckoned as the results influenced by both aerobic mineralization and $CaCO_3$ dissolution. Therefore, the influence of the two processes can be distinguished by pairwise comparison (Table 3).

In order to directly exhibit the change of the buffering capacity in different scenarios, we applied CO2SYS program (Lewis et al., 1998) to calculate H^+ and CO_2 concentrations from assumed seawater DIC and TA (Table 3) and depicted them in Figure 7. Notably, the absolute concentrations of H^+ and CO_2 are mainly determined by the initial concentrations of DIC and TA, not available as buffering capacity indicators. Hence, we focused on the concentration changes between these scenarios. At SSW-A, the TOC degradation increased CO_2 and H^+, leading to pH being lowered by 0.2; while when additional TA was involved, CO_2 and H^+ decreased by approximate 30%. Although the variation in different scenarios was not obvious at SSW-B as CO_2 and H^+ concentrations were high, the H^+ induced by TOC degradation was still slightly lowered by ~2% via adding extra TA. In contrast, the parameters at SSW-C kept consistent in the scenarios, indicating that the water was rarely influenced by benthic inputs. However, the absolute amount of TA added is not the primary factor in elevating pH. Although the TA level in seawater groups is elevated to a similar extent relative to the other two groups, the pH shows opposite response: the pH of seawater group is higher than that in the DIC-TOC-only group but lower than that in the no-efflux group.

https://doi.org/10.5194/egusphere-2026-3442
Preprint. Discussion started: 29 June 2026

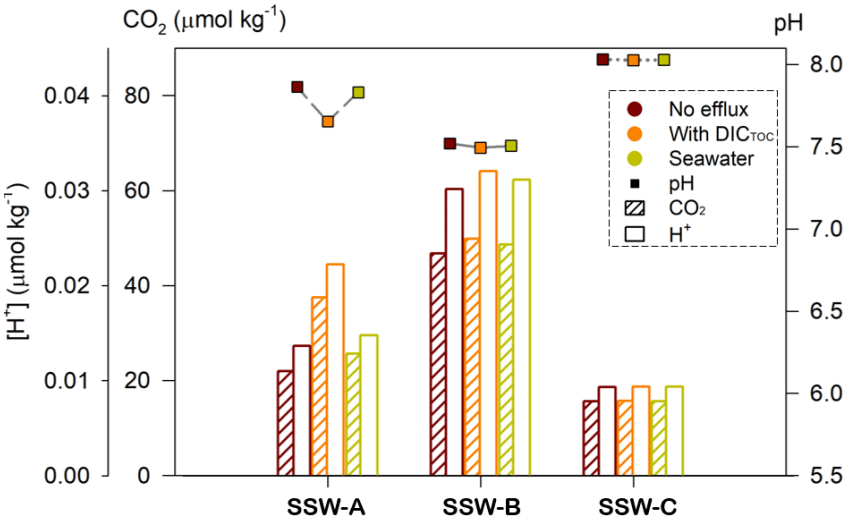

Figure 7: The variations of pH (plots), CO_2 (shadowed bars) and H^+ (filled bars) concentrations at each station in different scenarios which are shown in colors (red: without benthic input; orange: only with DIC derived from organic degradation; yellow: with all of benthic inputs). The axes on the left are for the bars and the right axis is for the plots.

Instead, the ratio of added TA and DIC (i.e., ΔTA/ΔDIC) is likely the determining factor for whether the acidification is mitigated. Thus, ΔTA/ΔDIC between seawater and other two groups (no-efflux and DIC-TOC-only) are calculated respectively and the results are shown in Table 3. When $\frac{\Delta TA}{\Delta DIC}>1$, pH increases and the extent of pH rise becomes larger with the increasing ratio. Conversely, when $\frac{\Delta TA}{\Delta DIC}<1$, pH exhibits a decreasing trend, and the variation in pH is primarily governed by the amount of DIC added to the system. Given that DIC release from organic carbon degradation is often inevitable in coastal seas, processes leading to $\frac{\Delta TA}{\Delta DIC}>1$ are critical to counteract the negative effects induced by excess DIC.

https://doi.org/10.5194/egusphere-2026-3442
Preprint. Discussion started: 29 June 2026

Table 3: The concentrations of TA and DIC in seawater influenced by different processes. The pH and CO_2 were calculated from the DIC and TA ahead using the CO2SYS program[#].

Station	Scenarios	TA ($\mu mol\ kg^{-1}$)	DIC ($\mu mol\ kg^{-1}$)	pH	CO_2 ($\mu mol\ kg^{-1}$)	$\frac{\Delta TA}{\Delta DIC}$
SSW-A	No benthic input	2201	2066	7.86	21.9	0.96[$]
	DIC-TOC only	2201	2137	7.65	37.5	2.18[*]
	Seawater	2357	2229	7.83	25.7	—
SSW-B	No benthic input	1973	1951	7.52	46.8	0.70[$]
	DIC-TOC only	1973	1958	7.49	49.9	1.27[*]
	Seawater	1982	1964	7.51	48.6	—
SSW-C	No benthic input	2241	2048	8.03	15.6	0.73[$]
	DIC-TOC only	2241	2050	8.03	15.8	0.99[*]
	Seawater	2243	2051	8.03	15.7	—

[#] The carbonic acid dissociation constants (K_1 and K_2) are from Lehrter et al. (2012), K_{HSO4} dissociation constants are from Dickson (1990), and total borate-salinity relationship is from Lee et al. (2010). All pH values are reported on the total hydrogen scale (pH_T).

[$] The ratio is calculated by comparing "No benthic input" and "Seawater" scenarios.

[*] The ratio is calculated by comparing "DIC-TOC only" and "Seawater" scenarios.

Early diagenetic processes in sediment generally exhibit specific $\frac{\Delta TA}{\Delta DIC}$ ratios like R1 and R2 if we assume that the composition of labile organic matter in the sediment follows the Redfield ratio (C:N:P = 106:16:1) (Middelburg et al., 2020). The $\frac{\Delta TA}{\Delta DIC}$ derived from aerobic mineralization and $CaCO_3$ dissolution, according to the stoichiometric amount of the reactions, are 0.14 and 2, respectively.

$OC + O_2 \rightarrow CO_2 + 16/106NH_3 + 1/106H_3PO_4$, $\frac{\Delta TA}{\Delta DIC} = (16/106 - 1/106)/1 = 0.14$ (R1)

$CaCO_3 + CO_2 \rightarrow Ca^{2+} + 2HCO_3^-$, $\frac{\Delta TA}{\Delta DIC} = 2/(2 - 1) = 2$ (R2)

Based on the contributions to DIC effluxes in Sect. 4.3, the TA release via sediment $CaCO_3$ dissolution (R2) was consequently approximately 678 ± 205, 185 ± 87.1 and 80.4 ± 20.9 mmol m^{-2} d^{-1} for SSW-A, SSW-B and SSW-C, respectively. These results are comparable with the benthic TA fluxes estimated from ^{224}Ra-^{228}Th disequilibria (see Table 2). Following the f_{CaCO_3}/f_{TOC} ratios (1.2, 0.8 and 0.4 for SSW-A/B/C) and the stoichiometry of R1 and R2, the theoretical F_{TA}/F_{DIC} ratios can be calculated as 1.16, 0.97 and

https://doi.org/10.5194/egusphere-2026-3442
Preprint. Discussion started: 29 June 2026

0.68 for SSW-A/B/C. In fact, the practical ratios for these sites were 0.95, 0.70 and 0.73, respectively (see Table 2). The lower practical F_{TA}/F_{DIC} ratios indicate that employing the average f_{CaCO_3}/f_{TOC} of the entire core introduced bias when quantifying process influences on benthic effluxes. Therefore, high-resolution f_{CaCO_3}/f_{TOC} ratios of surface sediment are essential in future studies to ensure accurate assessments.

Overall, $CaCO_3$ dissolution is the key process that enhanced TA and promoted the benthic F_{TA}/F_{DIC} above 1. As demonstrated by the scenario comparison, an addition with a high $\frac{\Delta TA}{\Delta DIC}$ ratio can effectively elevate the pH of water column, indicating that $CaCO_3$ dissolution is a viable approach to enhance the buffering capacity. In coastal seas where organic matter accumulation in sediments is high, this process serves as a vital regulator of the carbonate system in bottom water, mitigating the risk of acidification induced by organic matter degradation. Accordingly, the implementation of a co-culture model with shellfish is necessary in maricultural farms for additional $CaCO_3$ supply.

5 Conclusions

This study chose a coastal bay as a high-productivity representative and quantified the benthic processes affecting the carbonate system. Using the ^{224}Ra–^{228}Th disequilibrium approach, the highest fluxes of DIC and TA were found in the regions of seaweed farms, demonstrating that the benthic input accounted for the DIC and TA hotspots observed in water columns. Intensive bioturbation in the sediment and the hydrodynamics were confirmed to regulate the exchange across the sediment-water interface in the bay. Based on the $\delta^{13}C_{DIC}$ signatures of different sources, the roles of organic matter degradation and $CaCO_3$ dissolution in elevating porewater DIC concentrations were quantified. The results illustrated that $CaCO_3$ dissolution contributed 27–56% of the increased DIC in porewater and dominated the TA release from the sediment, balancing the H^+ increment induced by aerobic mineralization.

This research sheds light on the self-regulating mechanism of the carbonate system in a high-productivity coastal zone, and for the first time, illustrates the dynamic impact on sediment $CaCO_3$ dissolution: intensive disturbance affects the accumulation of metabolic CO_2 from organic carbon degradation, thereby influencing the extent of $CaCO_3$ dissolution. The benthic TA input from the sediment $CaCO_3$ dissolution is validated as a key role in maintaining the buffering capacity of seawater, lowering the potential acidification associated with the organic carbon remineralization. As biogenic $CaCO_3$ commonly exist in sediments, the sediment $CaCO_3$ dissolution was likely a ubiquitous process in the ocean, even in $CaCO_3$ supersaturated surroundings. This provides an insight into the carbon cycling of coastal and marginal seas that sediment $CaCO_3$ dissolution needs to be included in assessing the budget of inorganic carbon.

https://doi.org/10.5194/egusphere-2026-3442
Preprint. Discussion started: 29 June 2026

Appendix

Supporting information in appendix includes Tables S1 to S4 and Figures S1 to S3.

Code and data Availability

The sediment and porewater data, the R codes for statistical testing and analysis results are available through Mendeley Data, V2, doi: 10.17632/wd5xyszzjv.2.

Team list

Xinjie Ma, master student of Jimei University.

Xiangming Shi, associate professor of Jimei University.

Yingxu Wu, associate professor of Jimei University.

Xiangqi Yi, lecture of Jimei University.

Biqi Zheng, engineer of Chinese Ministry of Natural Resources.

Di Qi, professor of Jimei University.

CRediT authorship contribution statement

Xinjie Ma: Investigation, Methodology, Writing - Original Draft, Formal analysis. Xiangming Shi: Conceptualization, Investigation, Methodology, Data curation, Formal analysis, Writing - Original Draft, Writing - Reviewing and Editing, Funding acquisition. Yingxu Wu: Writing - Reviewing and Editing. Xiangqi Yi: Statistical Analysis, Writing - Reviewing and Editing. Biqi Zheng: Writing - Reviewing and Editing. Di Qi: Project administration, Writing - Reviewing and Editing, Supervision.

Conflict of Interest

The authors declare there are no conflicts of interest for this manuscript.

Disclaimer

Copernicus Publications remains neutral with regard to jurisdictional claims made in the text, published maps, institutional affiliations, or any other geographical representation in this paper. While Copernicus Publications makes every effort to include appropriate place names, the final responsibility lies with the authors. Views expressed in the text are those of the authors and do not necessarily reflect

https://doi.org/10.5194/egusphere-2026-3442
Preprint. Discussion started: 29 June 2026

the views of the publisher.

Acknowledgements

580 This study was supported by the Natural Science Foundation of Fujian Province (2023J01796), National Science Foundation of China (NSFC 42206042) and the Ocean Negative Carbon Emissions (ONCE) Program. The authors appreciate all members of the Polar and Marine Research Institute at Jimei University for their assistance in field sample collection and laboratory analysis.

https://doi.org/10.5194/egusphere-2026-3442
Preprint. Discussion started: 29 June 2026

References

Alling, V., Porcelli, D., Sanchez-Garcia, L., Gustafsson, O., Andersson, P. S., and Humborg, C.: Degradation of terrestrial organic carbon, primary production and out-gassing of CO_2 in the Laptev and East Siberian Seas as inferred from $\delta^{13}C$ values of DIC, Geochim. Cosmochim. Acta, 95, 143–159, https://doi.org/10/f22xrt, 2012.

Bauer, J. E., Cai, W.-J., Raymond, P. A., Bianchi, T. S., Hopkinson, C. S., and Regnier, P. A. G.: The changing carbon cycle of the coastal ocean, Nature, 504, 61–70, https://doi.org/10.1038/nature12857, 2013.

Berner, R. A.: Early diagenesis: a theoretical approach, Princeton University Press, https://doi.org/10.2307/j.ctvx8b6p2, 1980.

Boudreau, B. P., Middelburg, J. J., and Luo, Y.: The role of calcification in carbonate compensation, Nature Geosci, 11, 894–900, https://doi.org/10.1038/s41561-018-0259-5, 2018.

Burdige, D. J., Komada, T., Magen, C., and Chanton, J. P.: Modeling studies of dissolved organic matter cycling in Santa Barbara Basin (CA, USA) sediments, Geochim. Cosmochim. Acta, 195, 100–119, https://doi.org/10/f9jsjw, 2016.

Cai, P., Shi, X., Moore, W. S., and Dai, M.: Measurement of ^{224}Ra:^{228}Th disequilibrium in coastal sediments using a delayed coincidence counter, Mar. Chem., 138–139, 1–6, https://doi.org/10/g8wskm, 2012.

Cai, P., Shi, X., Hong, Q., Li, Q., Liu, L., Guo, X., and Dai, M.: Using $^{224}Ra/^{228}Th$ disequilibrium to quantify benthic fluxes of dissolved inorganic carbon and nutrients into the Pearl River Estuary, Geochim. Cosmochim. Acta, 170, 188–203, https://doi.org/10/f7z83x, 2015.

Cai, W.-J., Chen, F., Powell, E. N., Walker, S. E., Parsons-Hubbard, K. M., Staff, G. M., Wang, Y., Ashton-Alcox, K. A., Callender, W. R., and Brett, C. E.: Preferential dissolution of carbonate shells driven by petroleum seep activity in the Gulf of Mexico, Earth Planet. Sci. Lett., 248, 227–243, https://doi.org/10.1016/j.epsl.2006.05.020, 2006.

Dickson, A. G.: Standard potential of the reaction: $AgCl(s) + 12H_2(g) = Ag(s) + HCl(aq)$, and the standard acidity constant of the ion HSO_4^- in synthetic sea water from 273.15 to 318.15 K, J. Chem. Thermodyn., 22, 113–127, https://doi.org/10.1016/0021-9614(90)90074-Z, 1990.

https://doi.org/10.5194/egusphere-2026-3442
Preprint. Discussion started: 29 June 2026

Dickson, A. G., Afghan, J. D., and Anderson, G. C.: Reference materials for oceanic CO_2 analysis: a method for the certification of total alkalinity, Mar. Chem., 80, 185–197, https://doi.org/10.1016/S0304-4203(02)00133-0, 2003.

Duan, X., He, X., Chen, B., Gao, F., Cao, K., Lv, S., Tian, Y., Kong, X., Yin, P., Yang, L., and Xie, Y.: Significance of stable isotopic composition of dissolved inorganic carbon in the marginal seas of China, SSRN Electron. J., https://doi.org/10/g9mtd2, 2022.

Duarte, C. M., Delgado-Huertas, A., Marti, E., Gasser, B., Martin, I. S., Cousteau, A., Neumeyer, F., Reilly-Cayten, M., Boyce, J., Kuwae, T., Hori, M., Miyajima, T., Price, N. N., Arnold, S., Ricart, A. M., Davis, S., Surugau, N., Abdul, A.-J., Wu, J., Xiao, X., Chung, I. K., Choi, C. G., Sondak, C. F. A., Albasri, H., Krause-Jensen, D., Bruhn, A., Boderskov, T., Hancke, K., Funderud, J., Borrero-Santiago, A. R., Pascal, F., Joanne, P., Ranivoarivelo, L., Collins, W. T., Clark, J., Gutierrez, J. F., Riquelme, R., Avila, M., Macreadie, P. I., and Masque, P.: Carbon burial in sediments below seaweed farms matches that of Blue Carbon habitats, Nat. Clim. Change, 15, 180–187, https://doi.org/10.1038/s41558-024-02238-1, 2025.

FAO: The state of world fisheries and aquaculture 2024. Blue transformation in action, FAO, Rome, Italy, 264 pp., https://doi.org/10.4060/cd0683en, 2024.

https://doi.org/10.5194/egusphere-2026-3442
Preprint. Discussion started: 29 June 2026

Friedlingstein, P., O'Sullivan, M., Jones, M. W., Andrew, R. M., Hauck, J., Landschützer, P., Le Quéré, C., Li, H., Luijkx, I. T., Olsen, A., Peters, G. P., Peters, W., Pongratz, J., Schwingshackl, C., Sitch, S., Canadell, J. G., Ciais, P., Jackson, R. B., Alin, S. R., Arneth, A., Arora, V., Bates, N. R., Becker, M., Bellouin, N., Berghoff, C. F., Bittig, H. C., Bopp, L., Cadule, P., Campbell, K., Chamberlain, M. A., Chandra, N., Chevallier, F., Chini, L. P., Colligan, T., Decayeux, J., Djeutchouang, L. M., Dou, X., Duran Rojas, C., Enyo, K., Evans, W., Fay, A. R., Feely, R. A., Ford, D. J., Foster, A., Gasser, T., Gehlen, M., Gkritzalis, T., Grassi, G., Gregor, L., Gruber, N., Gürses, Ö., Harris, I., Hefner, M., Heinke, J., Hurtt, G. C., Iida, Y., Ilyina, T., Jacobson, A. R., Jain, A. K., Jarníková, T., Jersild, A., Jiang, F., Jin, Z., Kato, E., Keeling, R. F., Klein Goldewijk, K., Knauer, J., Korsbakken, J. I., Lan, X., Lauvset, S. K., Lefèvre, N., Liu, Z., Liu, J., Ma, L., Maksyutov, S., Marland, G., Mayot, N., McGuire, P. C., Metzl, N., Monacci, N. M., Morgan, E. J., Nakaoka, S.-I., Neill, C., Niwa, Y., Nützel, T., Olivier, L., Ono, T., Palmer, P. I., Pierrot, D., Qin, Z., Resplandy, L., Roobaert, A., Rosan, T. M., Rödenbeck, C., Schwinger, J., Smallman, T. L., Smith, S. M., Sospedra-Alfonso, R., Steinhoff, T., et al.: Global carbon budget 2024, Earth Syst. Sci. Data, 17, 965–1039, https://doi.org/10.5194/essd-17-965-2025, 2025.

Gillikin, D. P., Lorrain, A., Bouillon, S., Willenz, P., and Dehairs, F.: Stable carbon isotopic composition of *Mytilus edulis* shells: relation to metabolism, salinity, $\delta^{13}C_{DIC}$ and phytoplankton, Org. Geochem., 37, 1371–1382, https://doi.org/10/b9rbrv, 2006.

Glud, R. N., Berg, P., Stahl, H., Hume, A., Larsen, M., Eyre, B. D., and Cook, P. L. M.: Benthic carbon mineralization and nutrient turnover in a scottish sea loch: An integrative in situ study, Aquatic Geochemistry, 22, 443–467, https://doi.org/10.1007/s10498-016-9300-8, 2016.

Gran, G.: Determination of the equivalence point in potentiometric titrations. Part II, Analyst, 77, 661–671, https://doi.org/10.1039/AN9527700661, 1952.

Hadden, C. S., Loftis, K. M., and Cherkinsky, A.: Carbon Isotopes ($\delta^{13}C$ and $\Delta^{14}C$) in Shell Carbonate, Conchiolin, and Soft Tissues in Eastern Oyster (*Crassostrea Virginica)*, Radiocarbon, 60, 1125–1137, https://doi.org/10/gd9xww, 2018.

Harikrishnan, S. and Nathan, D. S.: Abundance and distribution of recent benthic foraminifera from the southwestern part of the Bay of Bengal, Geosyst. Geoenviron., 2, 100209, https://doi.org/10.1016/j.geogeo.2023.100209, 2023.

https://doi.org/10.5194/egusphere-2026-3442
Preprint. Discussion started: 29 June 2026

Hong, Q., Cai, P., Shi, X., Li, Q., and Wang, G.: Solute transport into the Jiulong River estuary via pore water exchange and submarine groundwater discharge: New insights from $^{224}Ra/^{228}Th$ disequilibrium, Geochim. Cosmochim. Acta, 198, 338–359, https://doi.org/10/f9js4s, 2017.

Hu, X. and Burdige, D. J.: Enriched stable carbon isotopes in the pore waters of carbonate sediments dominated by seagrasses: Evidence for coupled carbonate dissolution and reprecipitation, Geochim. Cosmochim. Acta, 71, 129–144, https://doi.org/10/cnngvm, 2007.

Hung, C.-C., Tseng, C.-W., Gong, G.-C., Chen, K.-S., Chen, M.-H., and Hsu, S.-C.: Fluxes of particulate organic carbon in the East China Sea in summer, Biogeosciences, 10, 6469–6484, https://doi.org/10.5194/bg-10-6469-2013, 2013.

Jahnke, R. A., Craven, D. B., and Gaillard, J.-F.: The influence of organic matter diagenesis on $CaCO_3$ dissolution at the deep-sea floor, Geochimica et Cosmochimica Acta, 58, 2799–2809, https://doi.org/10.1016/0016-7037(94)90115-5, 1994.

Jahnke, R. A., Craven, D. B., McCorkle, D. C., and Reimers, C. E.: $CaCO_3$ dissolution in California continental margin sediments: The influence of organic matter remineralization, Geochim. Cosmochim. Acta, 61, 3587–3604, https://doi.org/10/bc3xh4, 1997.

LaRowe, D. E., Arndt, S., Bradley, J. A., Burwicz, E., Dale, A. W., and Amend, J. P.: Organic carbon and microbial activity in marine sediments on a global scale throughout the quaternary, Geochim. Cosmochim. Acta, 286, 227–247, https://doi.org/10.1016/j.gca.2020.07.017, 2020.

Lee, K., Kim, T.-W., Byrne, R. H., Millero, F. J., Feely, R. A., and Liu, Y.-M.: The universal ratio of boron to chlorinity for the north pacific and north atlantic oceans, Geochim. Cosmochim. Acta, 74, 1801–1811, https://doi.org/10.1016/j.gca.2009.12.027, 2010.

Lehrter, J. C., Beddick, D. L., Devereux, R., Yates, D. F., and Murrell, M. C.: Sediment-water fluxes of dissolved inorganic carbon, O_2, nutrients, and N_2 from the hypoxic region of the Louisiana continental shelf, Biogeochemistry, 109, 233–252, https://doi.org/10/bd94ck, 2012.

Lewis, E., Wallace, D., and Allison, L. J.: Program developed for CO_2 system calculations, Brookhaven National Lab., Dept. of Applied Science, Upton, NY (United States); Oak Ridge National Lab., Carbon Dioxide Information Analysis Center, TN (United States), https://doi.org/10.2172/639712, 1998.

https://doi.org/10.5194/egusphere-2026-3442
Preprint. Discussion started: 29 June 2026

Lin, H., Chen, Z., Hu, J., Cucco, A., Zhu, J., Sun, Z., and Huang, L.: Numerical simulation of the hydrodynamics and water exchange in Sansha Bay, Ocean Eng., 139, 85–94, https://doi.org/10.1016/j.oceaneng.2017.04.031, 2017.

Lin, H., Chen, Z., Hu, J., Cucco, A., Sun, Z., Chen, X., and Huang, L.: Impact of cage aquaculture on water exchange in Sansha Bay, Cont. Shelf Res., 188, 103963, https://doi.org/10.1016/j.csr.2019.103963, 2019.

Liu, Y., Yang, W., Wu, Y., Cai, W.-J., Li, C., Lin, H., Zhuang, P., Zhang, J., Xu, Y., Qiu, H., Huang, Y., and Qi, D.: Emergent seasonal hypoxia and acidification risks induced by seaweed and fish polyculture in the world's largest seaweed farm, Limnol. Oceanogr. Lett., 10, 911–922, https://doi.org/10.1002/lol2.70055, 2025.

Mathis, M., Lacroix, F., Hagemann, S., Nielsen, D. M., Ilyina, T., and Schrum, C.: Enhanced CO_2 uptake of the coastal ocean is dominated by biological carbon fixation, Nat. Clim. Change, 14, 373–379, https://doi.org/10.1038/s41558-024-01956-w, 2024.

Middelburg, J. J.: Reviews and syntheses: To the bottom of carbon processing at the seafloor, Biogeosciences, 15, 413–427, https://doi.org/10.5194/bg-15-413-2018, 2018.

Middelburg, J. J., Soetaert, K., and Hagens, M.: Ocean Alkalinity, Buffering and Biogeochemical Processes, Rev. Geophys., 58, e2019RG000681, https://doi.org/10/gjp3s4, 2020.

Millero, F. J.: The marine inorganic carbon cycle, Chem. Rev., 107, 308–341, https://doi.org/10.1021/cr0503557, 2007.

Morse, J. W., Andersson, A. J., and Mackenzie, F. T.: Initial responses of carbonate-rich shelf sediments to rising atmospheric pCO_2 and "ocean acidification": Role of high Mg-calcites, Geochim. Cosmochim. Acta, 70, 5814–5830, https://doi.org/10.1016/j.gca.2006.08.017, 2006.

Ortega, T., Ponce, R., Forja, J., and Gomez-Parra, A.: Fluxes of dissolved inorganic carbon in three estuarine systems of the Cantabrian Sea (north of Spain), Journal of Marine Systems, 53, 125–142, https://doi.org/10.1016/j.jmarsys.2004.06.006, 2005.

R Core Team: R: A Language and Environment for Statistical Computing. R Foundation for Statistical Computing, Vienna, Austria URL https://www.R-project.org/, 2023

Seeberg-Elverfeldt, J., Schlüter, M., Feseker, T., and Kölling, M.: Rhizon sampling of porewaters near the sediment-water interface of aquatic systems, Limnol. Oceanogr. Methods, 3, 361–371, https://doi.org/10.4319/lom.2005.3.361, 2005.

https://doi.org/10.5194/egusphere-2026-3442
Preprint. Discussion started: 29 June 2026

Shi, X., Mason, R. P., Charette, M. A., Mazrui, N. M., and Cai, P.: Mercury flux from salt marsh sediments: Insights from a comparison between $^{224}Ra/^{228}Th$ disequilibrium and core incubation methods, Geochim. Cosmochim. Acta, 222, 569–583, https://doi.org/10/gc4brv, 2018.

Shi, X., Wei, L., Hong, Q., Liu, L., Wang, Y., Xueying Shi, Ying Ye, and Pinghe Cai: Large benthic fluxes of dissolved iron in China coastal seas revealed by $^{224}Ra/^{228}Th$ disequilibria, Geochimica et Cosmochimica Acta, 260, 49–61, 2019.

Silverberg, N., Sundby, B., Mucci, A., Zhong, S., Arakaki, T., Hall, P., Landén, A., and Tengberg, A.: Remineralization of organic carbon in eastern Canadian continental margin sediments, Deep Sea Res. Part II, 47, 699–731, https://doi.org/10/fbk553, 2000.

Sun, Z., Li, X., Ouyang, Z., Featherstone, C., Atekwana, E. A., Hussain, N., and Cai, W.: Simultaneous onboard analysis of seawater dissolved inorganic carbon (DIC) concentration and stable isotope ratio (δ^{13}C-DIC), Limnol. Oceanogr. Methods, 22, 862–875, https://doi.org/10.1002/lom3.10642, 2024.

Surge, D., Lohmann, K. C., and Dettman, D. L.: Controls on isotopic chemistry of the American oyster, *Crassostrea virginica*: implications for growth patterns, Palaeogeogr., Palaeoclimatol., Palaeoecol., 172, 283–296, https://doi.org/10/chhd5x, 2001.

Wakeham, S. G. and Canuel, E. A.: Degradation and Preservation of Organic Matter in Marine Sediments, in: Marine Organic Matter: Biomarkers, Isotopes and DNA, vol. 2N, edited by: Volkman, J. K., Springer-Verlag, Berlin/Heidelberg, 295–321, https://doi.org/10.1007/698_2_009, 2006.

Wang, A., Ye, X., Xu, X., Yin, X., and Xu, Y.: Settling flux and origin of particulate organic carbon in a macro-tidal semi-enclosed embayment: Luoyuan bay, southeast China coast, Estuar. Coast Shelf Sci., 206, 38–48, https://doi.org/10.1016/j.ecss.2017.03.023, 2018.

Wang, G., Han, A., Chen, L., Tan, E., and Lin, H.: Fluxes of dissolved organic carbon and nutrients via submarine groundwater discharge into subtropical Sansha Bay, China, Estuar. Coast Shelf Sci., 207, 269–282, https://doi.org/10/gd3rr7, 2018.

Wang, H., Dai, M., Liu, J., Kao, S.-J., Zhang, C., Cai, W.-J., Wang, G., Qian, W., Zhao, M., and Sun, Z.: Eutrophication-Driven Hypoxia in the East China Sea off the Changjiang Estuary, Environ. Sci. Technol., 50, 2255–2263, https://doi.org/10/f8cprr, 2016.

Wang, H., Teevan-Kamhawi, F., and Rebernik, O.: Harnessing nature's buffer: Assessing the role of bivalve shells in coastal alkalinity regeneration, Limnol. Oceanogr. Lett., 10, 774–781, https://doi.org/10.1002/lol2.70033, 2025.

https://doi.org/10.5194/egusphere-2026-3442
Preprint. Discussion started: 29 June 2026

Wang, N., Ji, W., Fu, J., and Zhou, J.: Community structure of macrobenthos and its relationship with mariculture in summer of Sansha Bay, Marine Fisheries, 41, 408–420, https://doi.org/10.13233/j.cnki.mar.fish.2019.04.003, 2019 (in Chinese).

Wang, Y., Yang, W., Zhao, X., Zhang, Q., Chen, H., Fang, Z., and Zheng, M.: Changes in the carbon source and storage in a cultivation area of macro-algae in Southeast China, Mar. Pollut. Bull., 188, 114680, https://doi.org/10.1016/j.marpolbul.2023.114680, 2023.

Ying, R., Monteiro, F. M., Wilson, J. D., Ödalen, M., and Schmidt, D. N.: Past foraminiferal acclimatization capacity is limited during future warming, Nature, 636, 385–389, https://doi.org/10.1038/s41586-024-08029-0, 2024.

Zhao, Y.: Organic carbon burial characteristics and the impact of offshore aquaculture in Sansha Bay, Fujian over the past century, thesis, East China Normal University, Shanghai, 86 pp., https://doi.org/10.27149/d.cnki.ghdsu.2023.002865, 2023 (in Chinese).